

*Article*

# The use of Semigeostrophic Theory to Diagnose the Behaviour of an Atmospheric GCM

Mike Cullen <sup>1,†,‡</sup> <sup>1</sup> Met Office; mike.cullen@metoffice.gov.uk [1]

† Current address: Met Office, Fitzroy Road, Exeter, EX1 3PB, UK

**Abstract:** A diagnostic method is presented for analysing the large-scale behaviour of the Met Office Unified Model, which is a comprehensive atmospheric model used for weather and climate prediction. Outside the boundary layer, on scales larger than the radius of deformation, semigeostrophic theory will give an accurate approximation to the model evolution. In particular, the ageostrophic circulation required to maintain geostrophic and hydrostatic balance against prescribed forcing and a rate of change of the geostrophic pressure can be calculated. In the tropics the balance condition degenerates to the weak temperature gradient approximation. Within the boundary layer the semigeostrophic approximation has to be used because friction and rotation are equally important. Assuming the calculated pressure tendency and ageostrophic circulation match the observed model behaviour, the influence of the large-scale state and the nature of the forcing on the model response can be deduced in a straightforward way. This process is illustrated by comparing predictions of the ageostrophic circulation from the theory and the model. It is then used to show that the effects of latent heat release can be included by modifying the static stability, and to show the effect of an idealised tropical heat source on the subtropical jet. Finally the response of the ageostrophic flow to boundary layer heating in the tropics is demonstrated. These illustrations show that the model behaviour on large scales conforms with theoretical expectations, so that the results of the diagnostic can be used to aid the development of further improvements to the model.

**Keywords:** Unified Model; geostrophic balance; geotriptic balance; ageotriptic circulation.

## 1. Introduction

In common with most other operational weather services and climate research centres, the Met Office uses a comprehensive atmospheric modelling system which is coupled to models of other parts of the Earth system, called the Unified Model (UM), [3]. In common with other centres, the Office undertakes a research programme aimed at improving the performance of the system. A particular focus is the study of systematic errors, where the Office uses a 'seamless' approach which exploits the fact that many such errors are present at different model resolutions and time periods, [17]. Typically the errors have large spatial scales. However, correcting them is not straightforward because of the strong coupling between atmospheric variables on large scales resulting from the requirements of geostrophic and hydrostatic balance. Near the equator, the geostrophic requirement degenerates to the 'weak temperature gradient' approximation (WTG), [22]. In the boundary layer, friction is also important leading to 'geotriptic' balance, [1]. This is particularly important in the tropics because it can support horizontal pressure and temperature gradients. The ageotriptic flow is strongly constrained by the need to maintain geotriptic and hydrostatic balance when the model is integrated in time. The result is that model changes which appear to be well-suited to reducing systematic errors may not have the intended effect.

In this paper, a diagnostic technique is proposed and illustrated which allows the geotriptic evolution and the ageotriptic circulation of the UM to be calculated for given data. The use of a decomposition of the UM fields into geotriptic and ageotriptic parts is only justified on scales larger

than the deformation radius, where the potential vorticity can be well approximated by a function of pressure. In this case, the pressure can be used as the controlling scalar variable and geotriptic winds and hydrostatic temperatures calculated from it. In three-dimensional flow, the requirement that the horizontal scale is greater than the deformation radius becomes a requirement that the aspect ratio is less than the ratio of the Coriolis and Brunt-Vaisala frequencies. The Lagrangian Rossby number also has to be small, restricting the curvature of trajectories. While these conditions appear very restrictive, they are also the conditions under which coherent anomalies are maintained. Near the equator, the decomposition is only justified outside the boundary layer for flows that are almost zonally symmetric and the WTG holds. These issues are discussed fully in [7]. Within the boundary layer, the usefulness of this method is greatly enhanced because horizontal pressure and temperature gradients can be supported. For instance, it was shown in [5] that using a SGT rather than a SG model allowed large-scale idealised cross-equatorial flows to be simulated.

The semi-geostrophic (SG) model was originally introduced by [11] as an alternative description of large-scale flows to the quasi-geostrophic model of [4]. It is based on what was subsequently called the Type II geostrophic scaling by [19] and in particular allows full variation of the static stability and Coriolis parameter. It is reviewed with a broader perspective by [12]. The model was then reintroduced by [14] to study frontogenesis. In that study a constant Coriolis parameter was used, which allows the equations to be transformed to a simpler form by using the geostrophic coordinate transformation. This version of the SG model can be solved for large times in isentropic coordinates by using optimal transport methods, as reviewed by [7]. Once the variable Coriolis parameter is included, the equations have to be solved in physical space. Formal arguments demonstrating how the equations can then be solved are given by [6] and [9]. However, the only rigorous result so far is limited to short times, and given by [10]. This result is sufficient to justify the diagnostic procedure used in this paper, where the equations are solved for a pressure tendency and ageostrophic wind at a single time in the manner of [20]. The extension to the semi-geotriptic (SGT) model is described by [1]. This is very important because it allows a realistic lower boundary condition. The need to use a nonlinear formulation of vertical momentum diffusion has meant that no rigorous treatment of this set of equations is yet available.

In the UM, the large-scale fields will be close to geotriptic and hydrostatic, so the ageotriptic circulation required to maintain this balance against forcing will be predicted by SGT theory. Thus if the UM forcing is diagnosed and input into the calculation of a single SGT timestep, the resulting ageotriptic flow should form a part of the ageotriptic flow actually produced by the UM. The total UM circulation will also contain transients, not subject to this constraint. In studying systematic UM errors, it is useful to determine what aspects of the circulation are constrained by the balance requirement, and which parts are evolving independently.

This calculation is a three-dimensional generalisation of the widely used Sawyer-Eliassen equation (SEE), e.g. [26]. An important feature of SEE is that the calculation of the ageostrophic circulation depends strongly on the static and inertial stability of the large-scale state. The effect of moisture on static stability can be included. Most of the applications of the SEE are in a vertical cross-section, where it is easy to justify its use. Examples specifically exploiting SG theory are [23] and [8]. Examples including the boundary layer using SGT theory are given by [1]. In three-dimensions, the validity of the SEE requires SG theory to be accurate, which implies the restrictions discussed above. This has limited its use.

In the next section the analytical formulation of the diagnostic is presented. The method works from the pressure field, which implies geotriptic winds and hydrostatic potential temperatures. As noted above, this is appropriate on scales where the SGT approximation is valid. However, UM data will contain non-geotriptic motions which affect the pressure, so steps have to be taken to minimise their effect on the diagnostic calculation. The equation for the pressure tendency is an elliptic equation, and the solution procedure is described. The discretisation of the equation requires care over orography, and it is essential to follow the principles of the UM scheme.

The results section includes four examples of the application of the diagnostic. The first is a comparison of the actual ageostriptic circulation produced by the UM in the extratropics with that calculated using SGT theory. This shows that the procedure is viable with full UM data subject to the extra processing noted in the previous paragraph. The second example calculates the vertical motion required to maintain large scale balance in cloudy air assuming moist static stability, and then inferring the latent heat release from the difference between the potential temperature increment calculated using this vertical motion with moist and dry static stability. This should represent the ‘forced’ part of the latent heating actually calculated by the UM physics. The third example shows the effect of an idealised tropical heat source on the extratropical flow following [15]. There is geostrophic adjustment in the north-south direction, as illustrated by [21], which should be realistic. The diagnostic also adjusts in the east-west direction, but except for very long forcing timescales this would in reality generate a tropical wave as in the simulations of [15] using an idealised general circulation model. The final example shows that thermally forced ageostriptic circulations in the boundary layer can be simulated.

## 2. Materials and Methods

### 2.1. The SG approximation to the UM equations equations

The diagnostic procedure uses the SGT and hydrostatic approximation to the deep atmosphere compressible equations solved by the UM, [25]. No other approximations are made, so that the diagnostic should extract the geotriptic part of the UM evolution.

We first write the equations in Lagrangian form. The equations are written in spherical polar and terrain-following coordinates  $(\lambda, \phi, \eta)$ , with the true radial coordinate  $r$ . The boundary layer momentum mixing is included, with stability dependent diffusion coefficient  $K_m$  as calculated by the UM. A derivative with respect to  $r$  is interpreted as a derivative with respect to  $\eta$  multiplied by  $\partial\eta/\partial r$  with  $(\lambda, \phi)$  constant.

$$\begin{aligned} \frac{D\mathbf{u}}{Dt} + c_{pd}\theta_v\nabla\pi + 2\Omega \times \mathbf{u} &= \mathbf{g} + \frac{\partial}{\partial r} \left( K_m \frac{\partial \mathbf{u}_h}{\partial r} \right) + S_{\mathbf{u}}, \\ \frac{D\theta_{vd}}{Dt} &= S_{\theta_{vd}}, \\ \frac{D\mu}{Dt} &= S_{\mu}, \\ \frac{\partial \rho_d}{\partial t} + \nabla \cdot (\rho_d \mathbf{u}) &= 0, \\ \rho_d &= \left( \frac{p_0}{R_d} \right) \frac{\pi^{\frac{1-\kappa_d}{\kappa_d}}}{\theta_{vd}}, \\ R_d &= \kappa_d c_{pd}, \\ \mu &= \sum m_X, X = v, cl, cf \dots, \\ \theta_v &= \frac{\theta_{vd}}{1 + \mu}. \end{aligned} \tag{1}$$

In these equations,  $\mathbf{u}$  is the vector velocity field and  $\theta_v$  the virtual potential temperature with  $\theta_{vd}$  the virtual potential temperature for dry air.  $\rho_d$  is the density of dry air and  $\pi$  the Exner pressure  $\left(\frac{p}{p_0}\right)^{\kappa_d}$ .  $p_0$  is a reference pressure,  $R_d$  is the gas constant for dry air and  $c_{pd}$  the specific heat of dry air at constant pressure.  $\kappa_d$  is defined by the penultimate equation of (1).  $m_X$  indicates the mixing ratio of various moisture constituents denoted by  $X$  and  $\mu$  is the sum of all these mixing ratios.  $\Omega$  is the Earth’s rotation vector and  $\mathbf{g}$  the gravitational and centrifugal vector.  $S_x$  is a source term for variable  $x$ . The suffix  $h$  denotes horizontal components.

The lower boundary condition is no slip. The upper boundary condition is a rigid lid.

The semi-geotriptic approximation in spherical geometry assumes first that the shallow atmosphere hydrostatic approximation holds, [24], so that the rotation term  $2\Omega \times \mathbf{u}$  is replaced by its horizontal components  $(-fv, fu)$  where  $f = 2\Omega \sin \phi$ , where  $\phi$  is the latitude, and that the gravitational vector  $\mathbf{g}$  only has a component in the local vertical. Then the vertical momentum equation in (1) becomes

$$c_{pd}\theta_v \frac{\partial \pi}{\partial r} = -g. \quad (2)$$

In order to understand the solutions, we subtract a reference state  $\pi_0(r)$  satisfying

$$c_{pd}\theta_0 \frac{\partial \pi_0}{\partial r} = -g, \quad (3)$$

where  $\theta_0$  is a constant, from  $\pi$  giving

$$c_{pd}\theta_v \frac{\partial \pi'}{\partial r} = g \frac{\theta'}{\theta_0}, \quad (4)$$

where  $\theta' = \theta_v - \theta_0$ . The Brunt-Vaisala frequency  $N$  is then given by

$$N^2 = \frac{g}{\theta_0} \frac{\partial \theta'}{\partial r}. \quad (5)$$

Assume typical scalings  $P$  and  $\Theta$  for  $\pi'$  and  $\theta'$ , ignore  $\mu$  and assume typical length scales  $L$  and  $H$  in the horizontal and vertical. Then  $\partial \pi' / \partial r \simeq P/H$  and the horizontal pressure gradient term  $\nabla_h \phi \simeq P/L$ . In some regimes the ratio of horizontal and vertical gradients of  $\pi'$  may be much less than  $H/L$  if  $\pi'$  is close to hydrostatic balance with a spatially uniform stably stratified reference profile  $\theta(r)$ . This is not generally the case on large scales with real data, particularly because of large horizontal variations of the tropopause height.

The geostrophic regime is characterised by the terms  $c_{pd}\theta_v \nabla_h \pi'$  in the horizontal momentum equations having the same magnitude as  $(-fv, fu)$ . Eqs. (4) and (5) show that  $c_{pd}\theta_v \partial \pi' / \partial r \simeq N^2 H$ . Defining  $U$  as a horizontal velocity scale, the geostrophic regime requires that  $fU \simeq N^2 H^2 / L$ . Now define the dimensionless Rossby and Froude numbers,  $Ro$  and  $Fr$  by

$$Ro = \frac{U}{fL}, Fr = \frac{U}{NH}, \quad (6)$$

Then geostrophic balance requires  $Ro = Fr^2$ . The semi-geostrophic regime is thus characterised by a small parameter  $\epsilon = Ro = Fr^2$ . The radius of deformation  $L_D$  is defined as  $NH/f$ , so that  $L/L_D = O(\epsilon^{-1/2})$ .

Geotriptic balance requires that the horizontal pressure gradient is comparable to the friction term. If  $K$  is a typical magnitude of the momentum diffusion coefficient  $K_m$ , this requires that  $N^2 H^2 / L \simeq KU/h^2$  where  $h \ll H$  is a typical boundary layer depth.. This scaling is discussed in [2].

Since the aim is to apply the diagnostic procedure directly to model data, the subtraction of a basic state as in (3) is not used. Therefore we define geotriptic and hydrostatic balance consistently with (1) by

$$\begin{aligned} c_{pd}\theta_v \nabla_h \pi - (fv_e, -fu_e) &= \frac{\partial}{\partial r} \left( K_m \frac{\partial \mathbf{u}_e}{\partial r} \right), \\ c_{pd}\theta_v \frac{\partial \pi}{\partial r} &= -g. \end{aligned} \quad (7)$$

Then the first equation of (1) can be approximated to  $O(\epsilon^2)$  outside the boundary layer by

$$\begin{aligned} \frac{D\mathbf{u}_e}{Dt} - f(v - v_e, u_e - u) &= \frac{\partial}{\partial r} \left( K_m \frac{\partial(\mathbf{u}_e - \mathbf{u}_\mu)}{\partial r} \right) + S_{\mathbf{u}}, \\ c_{pd}\theta_v \frac{\partial\pi}{\partial r} &= -g. \end{aligned} \quad (8)$$

(8) is only accurate to  $O(\epsilon)$  in the boundary layer, assuming  $h/H$  is independent of  $\epsilon$ . As discussed in [2], it is more typical for  $h/H$  to decrease with  $\epsilon$ , that paper suggests  $h/H \simeq \epsilon^{0.7}$ . The SGT approximation to (1) consists of (7), (8) and the equations of (1) after the first. The boundary conditions are the same as for (1).

## 2.2. The diagnostic equations

The diagnostic equations are based on the original equations (1). The equations are written in Eulerian form as in [20] so as to derive an Eulerian pressure tendency and an equation for the ageotropic winds. The first equation of (7) is written

$$\begin{aligned} f v_e + \frac{\partial}{\partial r} \left( K_m \frac{\partial u_e}{\partial r} \right) &= \frac{c_{pd}\theta_v}{r \cos \phi} \left( \frac{\partial\pi}{\partial\lambda} - \frac{\partial\pi}{\partial r} \frac{\partial r}{\partial\lambda} \right), \\ -f u_e + \frac{\partial}{\partial r} \left( K_m \frac{\partial v_e}{\partial r} \right) &= \frac{c_{pd}\theta_v}{r} \left( \frac{\partial\pi}{\partial\phi} - \frac{\partial\pi}{\partial r} \frac{\partial r}{\partial\phi} \right). \end{aligned} \quad (9)$$

(9) can be used to generate a single equation for  $u_e$  as follows:

$$\begin{aligned} f^2 u_e + \frac{\partial}{\partial r} \left( K_m \frac{\partial^2}{\partial r^2} \left( K_m \frac{\partial u_e}{\partial r} \right) \right) &= \\ \frac{\partial}{\partial r} \left( K_m \frac{\partial}{\partial r} \left( \frac{c_{pd}\theta_v}{r \cos \phi} \left( \frac{\partial\pi}{\partial\lambda} - \frac{\partial\pi}{\partial r} \frac{\partial r}{\partial\lambda} \right) \right) \right) &- f \frac{c_{pd}\theta_v}{r} \left( \frac{\partial\pi}{\partial\phi} - \frac{\partial\pi}{\partial r} \frac{\partial r}{\partial\phi} \right). \end{aligned} \quad (10)$$

Given values of  $\pi$ , (10) can be used to calculate  $v_e$ . The lower boundary condition is that  $u_e = v_e = 0$  at  $\eta = 0$ . It is assumed that  $K_m$  is zero above some  $\eta$  level below the upper boundary, so that setting  $K_m = 0$  there will generate an upper boundary condition for (10). For larger values of  $\eta$ , (10) can be solved independently at each level.

The first equation of (8) and the second and third equations of (1) can then be rewritten in Eulerian form as

$$\begin{aligned} \frac{\partial u_e}{\partial t} + \mathbf{u} \cdot \nabla u_e - f(v - v_e) &= \frac{\partial}{\partial r} \left( K_m \frac{\partial(u_e - u)}{\partial r} \right) + S_u, \\ \frac{\partial v_e}{\partial t} + \mathbf{u} \cdot \nabla v_e + f(u - u_e) &= \frac{\partial}{\partial r} \left( K_m \frac{\partial(v_e - v)}{\partial r} \right) + S_v, \\ \frac{\partial\theta_v}{\partial t} + \mathbf{u} \cdot \nabla\theta_v &= \frac{1}{1 + \mu} S_{\theta_{vd}} - \frac{\theta_{vd}}{(1 + \mu)^2} S_\mu \equiv S_{\theta_v}. \end{aligned} \quad (11)$$

Eq. (11) can be rewritten as

$$\mathbf{Q} \begin{pmatrix} u - u_e \\ v - v_e \\ w \end{pmatrix} + \frac{\partial}{\partial t} \begin{pmatrix} v_e \\ -u_e \\ \theta_v \end{pmatrix} = \mathbf{H}. \quad (12)$$

where

$$\mathbf{Q} = \begin{pmatrix} f + \frac{1}{r \cos \phi} \frac{\partial v_e}{\partial \lambda} + \frac{u_e \tan \phi}{r} & \frac{1}{r} \frac{\partial v_e}{\partial \phi} + \frac{\partial}{\partial r} \left( K_m \frac{\partial}{\partial r} \right) & \frac{\partial v_e}{\partial r} \\ -\frac{1}{r \cos \phi} \frac{\partial u_e}{\partial \lambda} + \frac{v_e \tan \phi}{r} - \frac{\partial}{\partial r} \left( K_m \frac{\partial}{\partial r} \right) & f - \frac{1}{r} \frac{\partial u_e}{\partial \phi} & -\frac{\partial u_e}{\partial r} \\ \frac{1}{r \cos \phi} \frac{\partial \theta_v}{\partial \lambda} & \frac{1}{r} \frac{\partial \theta_v}{\partial \phi} & \frac{\partial \theta_v}{\partial r} \end{pmatrix} \quad (13)$$

and

$$\mathbf{H} = \begin{pmatrix} -\mathbf{u}_e \cdot \nabla v_e + S_v \\ \mathbf{u}_e \cdot \nabla u_e - S_u \\ -\mathbf{u}_e \cdot \nabla \theta_v + S_{\theta_v} \end{pmatrix} \quad (14)$$

We now derive a single equation for the pressure tendency. Differentiating the second equation of (9) with respect to time gives

$$-f \frac{\partial u_e}{\partial t} + \frac{\partial}{\partial r} \left( K_m \frac{\partial}{\partial r} \left( \frac{\partial v_e}{\partial t} \right) \right) = \frac{c_{pd} \theta_v}{r} \frac{\partial}{\partial t} \left( \frac{\partial \pi}{\partial \phi} - \frac{\partial \pi}{\partial r} \frac{\partial r}{\partial \phi} \right) + \frac{1}{r} \left( \frac{\partial \pi}{\partial \phi} - \frac{\partial \pi}{\partial r} \frac{\partial r}{\partial \phi} \right) c_{pd} \frac{\partial \theta_v}{\partial t}. \quad (15)$$

Next define

$$\mathbf{B} = \begin{pmatrix} f & -\frac{\partial}{\partial r} \left( K_m \frac{\partial}{\partial r} \right) & 0 \\ \frac{\partial}{\partial r} \left( K_m \frac{\partial}{\partial r} \right) & f & 0 \\ 0 & 0 & g/\theta_v \end{pmatrix}. \quad (16)$$

Then using (9), the similar equation for  $\partial \pi / \partial \lambda$  and the relation

$$c_{pd} \theta_v \frac{\partial}{\partial t} \left( \frac{\partial \pi}{\partial r} \right) = -\frac{g}{\theta_v} \frac{\partial \theta_v}{\partial t}, \quad (17)$$

obtained by differentiating the second equation of (8) with respect to time, we can write

$$\mathbf{B} \begin{pmatrix} \frac{\partial v_e}{\partial t} \\ -\frac{\partial u_e}{\partial t} \\ -\frac{\partial \theta_v}{\partial t} \end{pmatrix} = c_{pd} \theta_v \frac{\partial}{\partial t} \begin{pmatrix} \frac{1}{r \cos \phi} \left( \frac{\partial \pi}{\partial \lambda} - \frac{\partial \pi}{\partial r} \frac{\partial r}{\partial \lambda} \right) \\ \frac{1}{r} \left( \frac{\partial \pi}{\partial \phi} - \frac{\partial \pi}{\partial r} \frac{\partial r}{\partial \phi} \right) \\ \frac{\partial \pi}{\partial r} \end{pmatrix} + \begin{pmatrix} \frac{1}{r \cos \phi} \left( \frac{\partial \pi}{\partial \lambda} - \frac{\partial \pi}{\partial r} \frac{\partial r}{\partial \lambda} \right) \\ \frac{1}{r} \left( \frac{\partial \pi}{\partial \phi} - \frac{\partial \pi}{\partial r} \frac{\partial r}{\partial \phi} \right) \\ 0 \end{pmatrix} c_{pd} \frac{\partial \theta_v}{\partial t}. \quad (18)$$

Using (9), the second term on the right hand side can be replaced by

$$\mathbf{B} \begin{pmatrix} \frac{v_e}{\theta_v} \frac{\partial \theta_v}{\partial t} \\ \frac{u_e}{\theta_v} \frac{\partial \theta_v}{\partial t} \\ 0 \end{pmatrix}$$

and so this term can be amalgamated with the left hand side giving

$$\mathbf{B} \begin{pmatrix} \frac{\partial v_e}{\partial t} - \frac{v_e}{\theta_v} \frac{\partial \theta_v}{\partial t} \\ -\frac{\partial u_e}{\partial t} + \frac{u_e}{\theta_v} \frac{\partial \theta_v}{\partial t} \\ -\frac{\partial \theta_v}{\partial t} \end{pmatrix} \quad \text{or} \quad \mathbf{B} \begin{pmatrix} \theta_v \frac{\partial}{\partial t} \left( \frac{v_e}{\theta_v} \right) \\ -\theta_v \frac{\partial}{\partial t} \left( \frac{u_e}{\theta_v} \right) \\ -\frac{\partial \theta_v}{\partial t} \end{pmatrix}$$

Using the third equation of (11), we can then rewrite (12)-(14) as

$$\mathbf{BQ}' \begin{pmatrix} u - u_e \\ v - v_e \\ w \end{pmatrix} + c_{pd}\theta_v \frac{\partial}{\partial t} \begin{pmatrix} \frac{1}{r \cos \phi} \left( \frac{\partial \pi}{\partial \lambda} - \frac{\partial \pi}{\partial r} \frac{\partial r}{\partial \lambda} \right) \\ \frac{1}{r} \left( \frac{\partial \pi}{\partial \phi} - \frac{\partial \pi}{\partial r} \frac{\partial r}{\partial \phi} \right) \\ \frac{\partial \pi}{\partial r} \end{pmatrix} = \mathbf{BH}' \quad (19)$$

where

$$\mathbf{Q}' = \begin{pmatrix} f + \frac{\theta_v}{r \cos \phi} \frac{\partial}{\partial \lambda} \left( \frac{v_e}{\theta_v} \right) + \frac{u_e \tan \phi}{r} & \frac{\theta_v}{r} \frac{\partial}{\partial \phi} \left( \frac{v_e}{\theta_v} \right) + \frac{\partial}{\partial r} \left( K_m \frac{\partial}{\partial r} \right) & \theta_v \frac{\partial}{\partial r} \left( \frac{v_e}{\theta_v} \right) \\ -\frac{\theta_v}{r \cos \phi} \frac{\partial}{\partial \lambda} \left( \frac{u_e}{\theta_v} \right) + \frac{v_e \tan \phi}{r} - \frac{\partial}{\partial r} \left( K_m \frac{\partial}{\partial r} \right) & f - \frac{\theta_v}{r} \frac{\partial}{\partial \phi} \left( \frac{u_e}{\theta_v} \right) & -\theta_v \frac{\partial}{\partial r} \left( \frac{u_e}{\theta_v} \right) \\ \frac{1}{r \cos \phi} \frac{\partial \theta_v}{\partial \lambda} & \frac{1}{r} \frac{\partial \theta_v}{\partial \phi} & \frac{\partial \theta_v}{\partial r} \end{pmatrix} \quad (20)$$

and

$$\mathbf{H}' = \begin{pmatrix} -(\mathbf{u}_e \theta_v) \cdot \nabla \left( \frac{v_e}{\theta_v} \right) + S_v - \frac{v_e S_{\theta_v}}{\theta_v} \\ (\mathbf{u}_e \theta_v) \cdot \nabla \left( \frac{u_e}{\theta_v} \right) - S_u + \frac{u_e S_{\theta_v}}{\theta_v} \\ -\mathbf{u}_e \cdot \nabla \theta_v + S_{\theta_v} \end{pmatrix} \quad (21)$$

We can then write  $\mathbf{BH}'$  as  $\mathbf{G}$  where

$$\mathbf{G} = \begin{pmatrix} -f \frac{u_e \theta_v}{r \cos \phi} \frac{\partial}{\partial \lambda} \frac{v_e}{\theta_v} - \frac{f u_e^2 \tan \phi}{r} - f \frac{v_e \theta_v}{r} \frac{\partial}{\partial \phi} \frac{v_e}{\theta_v} + f S_v - \frac{f v_e S_{\theta_v}}{\theta_v} - \frac{\partial}{\partial r} \left( K_m \frac{\partial}{\partial r} \left( \frac{u_e S_{\theta_v}}{\theta_v} \right) \right) \\ f \frac{u_e \theta_v}{r \cos \phi} \frac{\partial}{\partial \lambda} \frac{u_e}{\theta_v} - \frac{f u_e v_e \tan \phi}{r} + f \frac{v_e \theta_v}{r} \frac{\partial}{\partial \phi} \frac{u_e}{\theta_v} - f S_u + \frac{f u_e S_{\theta_v}}{\theta_v} - \frac{\partial}{\partial r} \left( K_m \frac{\partial}{\partial r} \left( \frac{v_e S_{\theta_v}}{\theta_v} \right) \right) \\ -\frac{u_e}{r \cos \phi} \frac{\partial \theta_v}{\partial \lambda} - \frac{v_e}{r} \frac{\partial \theta_v}{\partial \phi} + \frac{g S_{\theta_v}}{\theta_v} \end{pmatrix}. \quad (22)$$

Since  $\mathbf{B}$  and  $\mathbf{Q}$  involve values at adjacent levels, it is impractical to eliminate  $\mathbf{u}$  directly from (19) in order to solve for  $\frac{\partial \pi}{\partial t}$ . In order to solve (19) reasonably accurately, a preconditioning is required. In order to invert  $\mathbf{BQ}'$ . We therefore approximate  $\mathbf{BQ}'$  by an invertible matrix  $\mathbf{P}$ , so that (19) is replaced by

$$\mathbf{P} \begin{pmatrix} u - u_e \\ v - v_e \\ w \end{pmatrix} + c_{pd}\theta_v \frac{\partial}{\partial t} \begin{pmatrix} \frac{1}{r \cos \phi} \left( \frac{\partial \pi}{\partial \lambda} - \frac{\partial \pi}{\partial r} \frac{\partial r}{\partial \lambda} \right) \\ \frac{1}{r} \left( \frac{\partial \pi}{\partial \phi} - \frac{\partial \pi}{\partial r} \frac{\partial r}{\partial \phi} \right) \\ \frac{\partial \pi}{\partial r} \end{pmatrix} = \mathbf{G}, \quad (23)$$

where  $\mathbf{P} = \mathbf{P}_1 \mathbf{P}_2 \mathbf{P}_3$ .  $\mathbf{P}_1$  is given by

$$\mathbf{P}_1 = \begin{pmatrix} f^2 + \frac{\partial}{\partial r} \left( K_m \frac{\partial^2}{\partial r^2} \left( K_m \frac{\partial}{\partial r} \right) \right) & 0 & 0 \\ 0 & f^2 + \frac{\partial}{\partial r} \left( K_m \frac{\partial^2}{\partial r^2} \left( K_m \frac{\partial}{\partial r} \right) \right) & 0 \\ 0 & 0 & 1 \end{pmatrix} \quad (24)$$

$\mathbf{P}_2$  is given by

$$\mathbf{P}_2 = \begin{pmatrix} f^2 + \frac{f\theta_v}{r \cos \phi} \frac{\partial v_e}{\partial \lambda} + \frac{f u_e \tan \phi}{r} & \frac{f\theta_v}{r} \frac{\partial v_e}{\partial \phi} & f\theta_v \frac{\partial v_e}{\partial r} \\ -\frac{f\theta_v}{r \cos \phi} \frac{\partial u_e}{\partial \lambda} + \frac{f v_e \tan \phi}{r} & f^2 - \frac{f\theta_v}{r} \frac{\partial u_e}{\partial \phi} & -f\theta_v \frac{\partial u_e}{\partial r} \\ \frac{g}{r \cos \phi} \frac{\partial \theta_v}{\partial \lambda} & \frac{g}{r\theta_v} \frac{\partial \theta_v}{\partial \phi} & \frac{g}{\theta_v} \frac{\partial \theta_v}{\partial r} \end{pmatrix}, \quad (25)$$

and

$$\mathbf{P}_3 = \begin{pmatrix} f^{-2} & 0 & 0 \\ 0 & f^{-2} & 0 \\ 0 & 0 & 1 \end{pmatrix} \quad (26)$$

We next have to eliminate  $\mathbf{u}$  using the continuity equation and equation of state, which are the fourth and fifth equations of (1). In  $(\lambda, \phi, \eta)$  coordinates we have  $\mathbf{u} = (u, v, \dot{\eta})$  and

$$\dot{\eta} \frac{\partial r}{\partial \eta} = w - \frac{u}{r \cos \phi} \frac{\partial r}{\partial \lambda} - \frac{v}{r} \frac{\partial r}{\partial \phi}. \quad (27)$$

This can be rewritten as

$$\mathbf{R} \begin{pmatrix} u \\ v \\ w \end{pmatrix} = \begin{pmatrix} u \\ v \\ \dot{\eta} \end{pmatrix}.$$

The continuity equation then takes the form

$$\frac{\partial}{\partial t} \left( r^2 \rho_d \frac{\partial r}{\partial \eta} \right) + \frac{1}{\cos \phi} \left( \frac{\partial}{\partial \lambda} \left( r \rho_d u \frac{\partial r}{\partial \eta} \right) + \frac{\partial}{\partial \phi} \left( r \rho_d v \cos \phi \frac{\partial r}{\partial \eta} \right) + \frac{\partial}{\partial \eta} \left( r^2 \rho_d \dot{\eta} \frac{\partial r}{\partial \eta} \right) \right) = 0 \quad (28)$$

Now, applying the operator

$$\nabla \cdot r^2 \rho_d \frac{\partial r}{\partial \eta} \mathbf{R}$$

to (23) and using (28) gives

$$-\frac{\partial}{\partial t} \left( r^2 \rho_d \frac{\partial r}{\partial \eta} \right) + \nabla \cdot \left( r^2 \rho_d c_{pd} \theta_v \frac{\partial r}{\partial \eta} \mathbf{R} \mathbf{P}^{-1} \frac{\partial}{\partial t} (\nabla_r \pi) \right) = \nabla \cdot \left( r^2 \rho_d \frac{\partial r}{\partial \eta} \mathbf{R} \mathbf{P}^{-1} \mathbf{G} \right) + \frac{1}{\cos \phi} \left( \frac{\partial}{\partial \lambda} \left( r \rho_d u_e \frac{\partial r}{\partial \eta} \right) + \frac{\partial}{\partial \phi} \left( r \rho_d v_e \cos \phi \frac{\partial r}{\partial \eta} \right) \right) \quad (29)$$

Next, differentiating the equation of state with respect to time gives

$$\frac{\kappa_d - 1}{\kappa_d} \pi^{-\frac{1}{\kappa_d}} \frac{\partial \pi}{\partial t} \rho_d \theta_{vd} + \pi^{\frac{\kappa_d - 1}{\kappa_d}} \frac{\partial \rho_d}{\partial t} \theta_{vd} + \pi^{\frac{\kappa_d - 1}{\kappa_d}} \rho_d \frac{\partial \theta_{vd}}{\partial t} = 0. \quad (30)$$

Removing common factors, and using equations (17) and the third equation of (1) to evaluate the final term gives

$$\frac{\kappa_d - 1}{\kappa_d} \frac{\partial \pi}{\partial t} \rho_d \theta_{vd} + \pi \frac{\partial \rho_d}{\partial t} \theta_{vd} - \pi \rho_d \frac{c_{pd} \theta_v^2}{g} \frac{\partial}{\partial t} \left( \frac{1}{(1 + \mu)} \frac{\partial \pi}{\partial r} \right) = 0. \quad (31)$$

We now substitute (31) into (29) to give

$$\begin{aligned} & \frac{\kappa_d - 1}{\kappa_d} \frac{\rho_d}{\pi} r^2 \frac{\partial r}{\partial \eta} \frac{\partial \pi}{\partial t} + r^2 \frac{\partial r}{\partial \eta} \frac{\rho_d c_{pd} \theta_v^2}{g \theta_{vd}} \frac{\partial}{\partial t} \left( \frac{1}{(1 + \mu)} \frac{\partial \pi}{\partial r} \right) + \\ \nabla \cdot & \left( r^2 \rho_d c_{pd} \theta_v \frac{\partial r}{\partial \eta} \mathbf{RP}^{-1} \frac{\partial}{\partial t} (\nabla_r \pi) \right) = \nabla \cdot \left( r^2 \rho_d \frac{\partial r}{\partial \eta} \mathbf{RP}^{-1} \mathbf{G} \right) + \\ & \frac{1}{\cos \phi} \left( \frac{\partial}{\partial \lambda} \left( r \rho_d u_e \frac{\partial r}{\partial \eta} \right) + \frac{\partial}{\partial \phi} \left( r \rho_d v_e \cos \phi \frac{\partial r}{\partial \eta} \right) \right). \end{aligned} \quad (32)$$

Apart from the small term  $\frac{\partial}{\partial t} \frac{1}{(1 + \mu)}$ , which needs to be diagnosed separately, this is an elliptic equation for  $\partial \pi / \partial t$ , which can be solved. Boundary conditions are required at the top and bottom. The boundary conditions inherited from (1) imply that  $\dot{\eta} = 0$  at the top and bottom, which implies a zero gradient of

$$r^2 \rho_d c_{pd} \theta_v \frac{\partial r}{\partial \eta} \mathbf{RP}^{-1} \frac{\partial}{\partial t} (\nabla_r \pi). \quad (33)$$

Eq. (27) and the no slip lower boundary condition then implies that  $w = 0$  at the lower boundary also. Then (19) and (21) reduce to

$$c_{pd} \theta_v \frac{\partial \pi}{\partial r} = S^{\theta_v}. \quad (34)$$

We can then calculate  $u - u_e, v - v_e$  and  $w$  from (23).

### 2.3. Application

The right hand side of (32) shows that the evolution is driven by the divergence of the forcing vector  $\mathbf{G}$  and the divergence of the geotriptic wind  $(u_e, v_e)$ . Changes to the forcing with zero divergence, in the sense of the first term on the right hand side of (32), will not affect the evolution. Such changes will simply alter the ageostrophic wind vector  $(u - u_e, v - v_e, w)$  so that (19) is satisfied. This demonstrates that changes to the forcing in the UM may have a much smaller effect on the large-scale evolution than might be expected.

Using the definition of  $\mathbf{G}$  in (22), we see that the first term on the right hand side of (32) includes geotriptic advection of the momentum and potential temperature, the dynamical forcing, together with the external forcing terms  $S$  which are generated by the UM physics. The second term on the right hand side would be just the divergence of the geostrophic wind if the boundary later were not included. This would be zero in pressure coordinates with a constant Coriolis parameter. There is a contribution from variations in the Coriolis parameter, which gives the effect of Rossby wave propagation on the pressure tendency. Since the divergence calculation used to derive (32) is in terrain-following coordinates, the orography will also contribute to this term through the horizontal variations of  $\frac{\partial r}{\partial \eta}$ . This shows how the orography can have a strong effect on the large-scale flow.

Moisture will interact strongly with the diagnostic procedure through the reduction of the effective static stability by latent heat release. In the UM, the thermodynamic equation, which is the second equation of (1), includes the terms

$$w \frac{\partial \theta_{vd}}{\partial r} = S_{LH},$$

where  $S_{LH}$  is the part of the forcing term resulting from latent heat release. This term is dominated by the term  $\frac{Dq_{sat}}{Dt}$ , where  $q_{sat}$  is the saturated mixing ratio which is largely a function of temperature. In a simple form, this can be represented by calculating a cloud fraction weighted static stability, where  $\partial \theta_{vd} / \partial r$  is the dry stability and  $\partial \theta_e / \partial z$  is the moist stability, where  $\theta_e$  is the equivalent potential temperature calculated assuming saturation.  $w$  is not known in advance, so the idea that latent heating only occurs with upward motion cannot be used as the problem becomes nonlinear in  $w$ . The use

of cloud fraction weighting avoids this problem, as evaporation will occur if  $w$  is negative in cloudy regions. If  $\alpha$  is the cloud fraction, we set

$$\left(\frac{\partial\theta_v}{\partial r}\right)_{eff} = \frac{\partial(\alpha\theta_e + (1-\alpha)\theta)}{\partial r}, \quad (35)$$

A more sophisticated approach would be to use a formula set out in [13] for wave propagation in inhomogeneous media. Applying this to a wet/dry mixture gives a modified Brunt-Vaisala frequency as

$$N_{eff}^2 = \left(\frac{\alpha N_d^2 + (1-\alpha)N_w^2}{N_w^2 N_d^2}\right)^{-1}, \quad (36)$$

where

$$N_w^2 = \frac{g}{\theta} \frac{\partial\theta_e}{\partial r}, N_d^2 = \frac{g}{\theta_{vd}} \frac{\partial\theta_{vd}}{\partial r}. \quad (37)$$

We thus replace  $\frac{\partial\theta_v}{\partial r}$  in  $\mathbf{Q}'$ , eq. (20), by

$$\left(\frac{\partial\theta_{vd}}{\partial r}\right)_{eff} = \left(\frac{\alpha \frac{\partial\theta_{vd}}{\partial r} + (1-\alpha) \frac{\partial\theta_e}{\partial r}}{\frac{\partial\theta_e}{\partial z} \frac{\partial\theta_{vd}}{\partial r}}\right)^{-1}. \quad (38)$$

The model value of cloud fraction  $\alpha$  can be used, provided again that small space and time scales are excluded.

If the temperature increment  $S_L$  from the large scale precipitation scheme is added to  $S$ , the solution of (19) will become

$$\mathbf{BQ}' \begin{pmatrix} u - u_e \\ v - v_e \\ w \end{pmatrix} + c_{pd}\theta_v \frac{\partial}{\partial t} \begin{pmatrix} \frac{1}{r \cos \phi} \left( \frac{\partial\pi}{\partial\lambda} - \frac{\partial\pi}{\partial r} \frac{\partial r}{\partial\lambda} \right) \\ \frac{1}{r} \left( \frac{\partial\pi}{\partial\phi} - \frac{\partial\pi}{\partial r} \frac{\partial r}{\partial\phi} \right) \\ \frac{\partial\pi}{\partial r} \end{pmatrix} = \mathbf{B} \left( \mathbf{H}' + \begin{pmatrix} 0 \\ 0 \\ S_L \end{pmatrix} \right). \quad (39)$$

The solution of (39) for  $\frac{\partial\pi}{\partial t}$  is identical to that of (19) if the element  $\frac{\partial\theta_v}{\partial r}$  in  $\mathbf{Q}'$  in that equation is replaced by  $\left(\frac{\partial\theta}{\partial r}\right)_{eff}$  as in (38) and

$$S_L = w \left( \frac{\partial\theta}{\partial z} - \left(\frac{\partial\theta}{\partial z}\right)_{eff} \right). \quad (40)$$

This will be approximately true if the latent heat release is dominated by the effects of vertical motion. This is illustrated in section 3.3.

#### 2.4. Computational aspects

The elliptic equation (32) is solved by a preconditioned generalised conjugate residual method which requires explicit evaluation of the elliptic operator on the left hand side for a given estimate of  $\partial\pi/\partial t$ , and an evaluation of the right hand side. The preconditioning is done by a vertical matrix inversion, which uses a tridiagonal solver, and a horizontal smoother.

Given  $\pi, K_m$  from model data, solve (10) and (9) for  $(u_e, v_e)$ . Care has to be taken in calculating the right hand side of (9) because the two terms cancel strongly over orography. The scheme, based on that used in the UM and exploiting hydrostatic balance, is

$$\frac{c_{pd}\theta_v}{r \cos \phi} \left( \frac{\partial\pi}{\partial\lambda} - \frac{\partial\pi}{\partial r} \frac{\partial r}{\partial\lambda} \right) \simeq c_{pd}\bar{\theta}_v^\lambda \delta_\lambda \pi + g\delta_\lambda r, \quad (41)$$

where  $\delta_\lambda$  indicates a central difference in the  $\lambda$  direction divided by  $2r \cos \phi \delta \lambda$ . A similar scheme is used in the  $\phi$  direction. Solving (10) then involves inverting a  $N \times N$  pentadiagonal matrix at each horizontal gridpoint. where  $N$  is the number of model levels where  $K_m$  is nonzero.

Next use  $(u_e, v_e)$  to evaluate the components of  $\mathbf{P}_2$ , (25). Central differencing has to be used because the upwind direction is not known in advance. The vertical stability is evaluated more accurately as a vertical second difference of  $\pi$ . The values are filtered towards a zonal mean close to the equator in order to remain within the validity of the theory. If equations (35) or (38) are used, the relative humidity, moisture content and cloud fraction are used to calculate the effective static stability.

Next calculate the eigenvalues of  $\mathbf{P}_2$  at each point. Modify  $\mathbf{P}_2$  as necessary to remove negative eigenvalues. This can be done by first replacing any negative diagonal terms by suitable reference values, such as  $10^{-10}$  in the first two rows and  $10^{-6}$  in the third, and then rescaling the off-diagonal terms as required.

Next construct the vertical preconditioner. If  $\mathbf{P}_{2ij}$  is the value of the  $(i, j)$  component of  $\mathbf{P}_2$ , calculate the rms value  $\mathbf{PI}_{rms}$  of  $\mathbf{P}_{233}^{-1}$  as a function of model level. Then at each horizontal gridpoint we precondition eq. (32) by replacing the left hand side by

$$\mathbf{A} \frac{\partial \pi}{\partial t} \equiv C_1 * \frac{\kappa_d - 1}{\kappa_d} \frac{\rho_d}{\pi} r^2 \frac{\partial r}{\partial \eta} \frac{\partial \pi}{\partial t} + \nabla \cdot \left( r^2 \rho_d c_{pd} \theta_v \frac{\partial r}{\partial \eta} \mathbf{RPI}_v \frac{\partial}{\partial t} (\nabla_r \pi) \right). \quad (42)$$

$C_1$  is set to 100 in the examples illustrated.  $\mathbf{PI}_v$  is a tridiagonal matrix at each gridpoint defined as

$$\mathbf{PI}_v = C_2 \mathbf{PI}_{rms} + (\mathbf{P}_{211}^{-1} + \mathbf{P}_{222}^{-1}). \quad (43)$$

$C_2$  is a matrix  $\begin{pmatrix} 1 & 0 & 0 \\ 0 & C_2 & 0 \\ 0 & 0 & 1 \end{pmatrix}$ , with  $C_2$  set to 1.5 in the examples illustrated.

Now solve (32) for  $\frac{\partial \pi}{\partial t}$  preconditioned with  $\mathbf{A}^{-1}$  as defined in (42) using a generalised conjugate residual method. Back substitute in (32) with the left hand side modified to

$$\frac{\kappa_d - 1}{\kappa_d} \frac{\rho_d}{\pi} r^2 \frac{\partial r}{\partial \eta} \frac{\partial \pi}{\partial t} + r^2 \frac{\partial r}{\partial \eta} \frac{\rho_d c_{pd} \theta_v^2}{g \theta_{vd}} \frac{\partial}{\partial t} \left( \frac{1}{(1 + \mu)} \frac{\partial \pi}{\partial r} \right) + C_3 \nabla \cdot \left( r^2 \rho_d c_{pd} \theta_v \frac{\partial r}{\partial \eta} \mathbf{RPI}_v^{-1} \frac{\partial}{\partial t} (\nabla_r \pi) \right). \quad (44)$$

$C_3$  is a constant set to 1.2 in the examples illustrated. Carry out iterations till the convergence slows (25 in the examples illustrated).

Now back substitute in (32) and calculate a residual. Repeat the inner iterations. This outer iteration was run 10 times in the examples illustrated. Finally use (23) to obtain  $\mathbf{u}$ . It is not currently practical to iterate this procedure further to solve (19) exactly

### 3. Results

#### 3.1. Experimental setup

The diagnostic can be calculated from UM data with whatever resolution is to be studied. In the examples quoted here, this was on a latitude longitude grid with  $640 \times 480$  points, with a north-south gridlength of about 40km. The data has 70 levels extending to 80km. The diagnostic is run on a grid of  $160 \times 120$  points, giving a north-south gridlength of about 125km, but the same levels as the UM. The illustrations use a single case from February 2014.

This procedure allows reasonable computational accuracy in computing scales of 500km or greater. However, it will still capture variability on scales smaller than where the SGT approximation is valid. Therefore the forcing fields are further smoothed. The coefficients of the  $\mathbf{Q}'$  matrix calculated from the

data will also emphasise smaller scales because of the derivatives used to define the coefficients. These are also smoothed. Near the equator an additional filter is applied to the geostrophic winds which relaxes them towards the zonal mean. This is needed because of the severe restrictions on the validity of SGT in the tropics outside the boundary layer.

### 3.2. Comparison of diagnostic and model-derived ageostrophic winds

Root mean square values of the geostrophic wind are about  $21\text{ms}^{-1}$  for this data, and root mean square values of the ageostrophic wind are about  $6.3\text{ms}^{-1}$ , giving a global averaged Rossby number of about 0.3. This would suggest a 10% expected error in the difference between the model wind and the total wind deduced from (19). The actual global rms difference between the diagnosed wind and the model wind is  $9.7\text{ms}^{-1}$  in an overall rms wind of  $22\text{ms}^{-1}$ . The global rms difference between the calculated geostrophic wind and the model wind is  $7.3\text{ms}^{-1}$ .

To illustrate this, Figure 1 shows a mid-tropospheric zonal geostrophic wind calculated using (9) and (10) from UM pressure and potential temperature fields. The area illustrated is the extratropical North Atlantic, so away from significant topography. It would be reasonable to expect the ageostrophic wind to be accurate over such an area. Fig. 1 shows the ageostrophic wind calculated from (19) and the difference between the UM wind and the geostrophic wind deduced from the pressure and temperature. There is a reasonable match between the two estimates of the ageostrophic wind, indicating that SGT theory is working reasonably accurately for the UM fields over the area chosen. The correlation coefficient between the two estimates of the ageostrophic wind is 0.69 over the area and level illustrated. This both illustrates the applicability of the theory and the ability of the UM to reproduce it.

The rms difference between the diagnosed wind and the model wind over the area and level shown in Fig. 1 is  $4.5\text{ms}^{-1}$  in an overall rms wind of  $22\text{ms}^{-1}$ , so the proportional error is 20% rather than 45% globally. The rms difference between the calculated geostrophic wind and the model wind is also about  $4.5\text{ms}^{-1}$ . Fig. 1 shows that the diagnosed ageostrophic wind is larger than the model value in some regions. This is typical of situations where the space or time scale is becoming too small for SGT theory to be accurate, and leads to the rms difference between the diagnosed wind and the model wind being no smaller than that between the calculated geostrophic wind and the model wind.

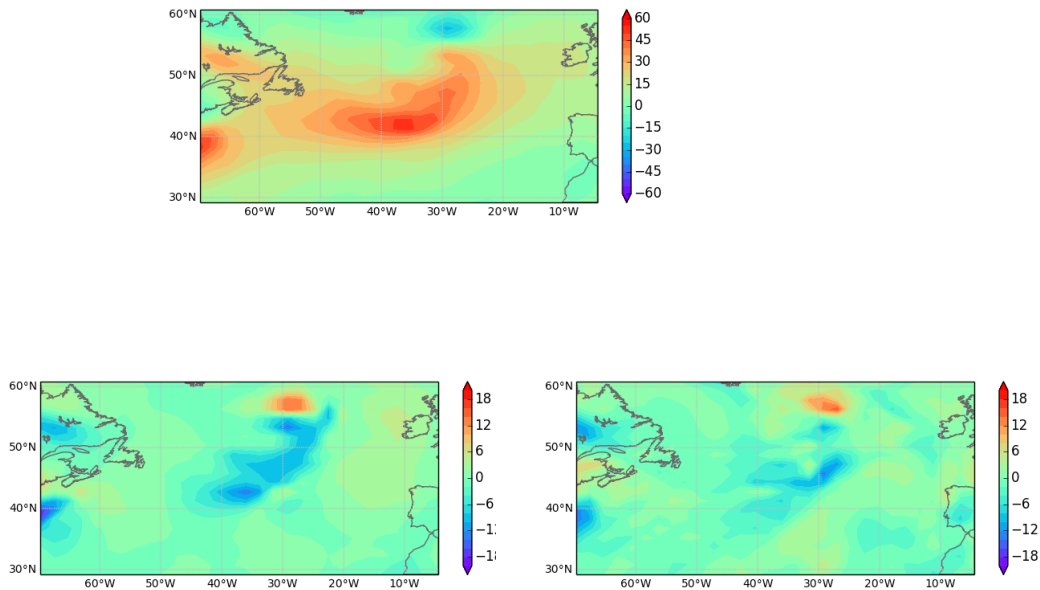


**Figure 1.** Zonal component of wind at 4000m, units  $\text{ms}^{-1}$ . (a) Geotriptic wind calculated from (9), (b) ageotriptic wind from (19), (c) ageotriptic wind from UM output.

### 3.3. Use of a modified static stability to represent latent heat release

In section 2.3 it is shown that the latent heating resulting from maintenance of geotriptic balance in cloudy airt can be deduced by solving (19) with a modified static stability as in (38). The resulting  $w$  can then be used in (40) to deduce the latent heating. This can be compared with the temperature increments from the schemes representing cloud and precipitation, both convective and dynamic, in the UM.

The results are shown in Fig 2. The area chosen is again the extratropical North Atlantic, so it can be expected that the vertical motion required to maintain geotriptic balance will be similar to that generated by the UM, and that precipitation processes, which generate most of the latent heating, will be strongly linked to the vertical velocity. In the first two panels the vertical velocity  $w$  diagnosed from (19) with (38) is compared with that directly output from the UM. As in the comparison of ageotriptic winds in Fig 1, there is reasonable agreement. In the second pair of panels, the latent heating deduced from (40) is compared with the temperature increments from the large-scale cloud scheme and the convection scheme combined. There is a strong correspondence between the diagnosed latent heating and the diagnosed vertical motion, as would be expected from (38). The correspondence between the model vertical motion and the model latent heating does not look as strong. However, the correlation coefficient between them for the plotted area and level is again 0.69. The visual mismatch is primarily because there is no latent heating in areas of downward motion. The diagnostic procedure will generate latent cooling in cloudy air, but this would result in rapid dissipation of the cloud and not correspond to significant latent cooling in the UM.

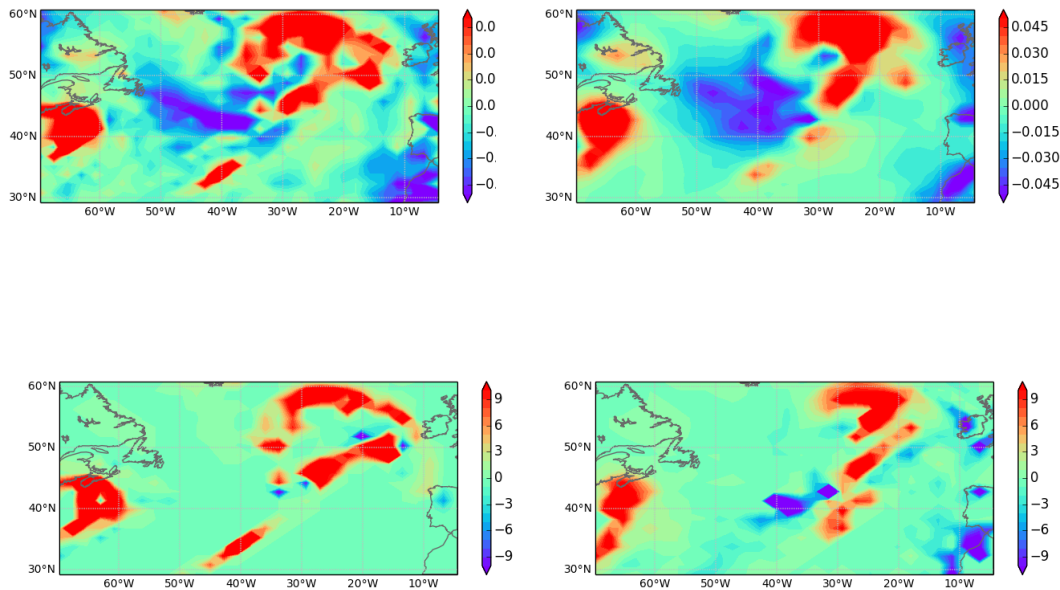


**Figure 2.** Vertical velocity at 4000m, units  $\text{ms}^{-1}$ : (a) directly output from UM, (b) calculated from (19). Heating rates at 4000m, units  $^{\circ}\text{K day}^{-1}$ : (c) combined heating from precipitation schemes in UM, (d) latent heating deduced as in section 2.3 (see text).

### 3.4. Effect of tropical heating on the subtropical jet

The diagnostic procedure can be applied using artificial physical forcing as well as that derived from the model. There has been considerable interest in the effect of tropical heating on the extratropical circulation. An example is the paper by Matthews *et al.* [18], where time dependent heating deduced from reanalyses is used to determine the response to forcing of a simple general circulation model (GCM) using a climatological mean state. This is compared with the observed evolution deduced from satellite data.

The diagnostic presented here calculates the ‘instant’ response of the geostrophic flow to forcing at a particular time. It is thus easiest to compare it with the earlier study of [15]. In that paper, the forcing was maintained over a long timescale, and an actual atmospheric state as well as a climatological state could be used to determine the response to the forcing. The atmospheric state was maintained in time by using an artificial forcing term. We apply a forcing similar to [15] and calculate the instant geostrophic response to this forcing using the atmospheric state illustrated in the rest of the paper. In [15], Fig. 17c shows the divergent response to the forcing, which is set up very quickly. This should be reproduced by the diagnostic. Fig. 18c also shows a significant downstream response at about  $30^{\circ}\text{N}$  in the subtropical jet after 5 days. Since Fig. 17c shows that the divergent response does not propagate much downstream, the formula for the source term plotted in Fig. 18c shows that this must represent a perturbation vorticity. Thus in our diagnostic we look for a localised perturbation to the geostrophic flow in the subtropical jet, which would then propagate downstream over the 5 day period illustrated by [15].

The heating in the mid troposphere is illustrated in Fig 3a. It is centred on the dateline as in [15], Fig. 17c. The heating extends through the troposphere. The zonal geostrophic wind is shown in Fig. 3b in the upper troposphere, noting that strong filtering has been applied near the equator to eliminate values for which SGT theory is inappropriate. The diagnosed zonal geostrophic wind tendency is shown in Fig. 3c. This peaks at the same longitude as the forcing, so would propagate the jet forwards.

The values peak at about  $0.5^{\circ}\text{K day}^{-1}$ . If this is applied over 15 days, this gives a similar impact to that shown in Fig. 12a of [15]. There are also impacts at lower latitudes, but these are not likely to be physically correct as they are outside the validity of SGT.

The reason for the strong interaction with the subtropical jet can be seen in Fig. 3d. This plots the second diagonal element of the matrix  $\mathbf{BQ}'$  defined in (16) and (20). In the absence of the non-trivial model state this would take the value  $f^2$ , about  $0.5_{10} - 8$  at  $30^{\circ}\text{N}$ . It can be seen that on the southern flank of the jet, where there is strong anticyclonic shear, the values drop to well below this. The effect can be seen from (19). If the matrix  $\mathbf{Q}'$  has a small eigenvalue, there will be a very strong response to forcing in this direction, so that in the present case there is a very efficient transfer of information from the heating to the subtropical jet. Comparing Figs. 3a and c shows that the largest impact is to the west of the forcing longitude, where the matrix coefficient is smallest. The diagnostic can thus pick up sensitivity of the response to forcing to the structure of the basic state, which is a topic of wide interest..

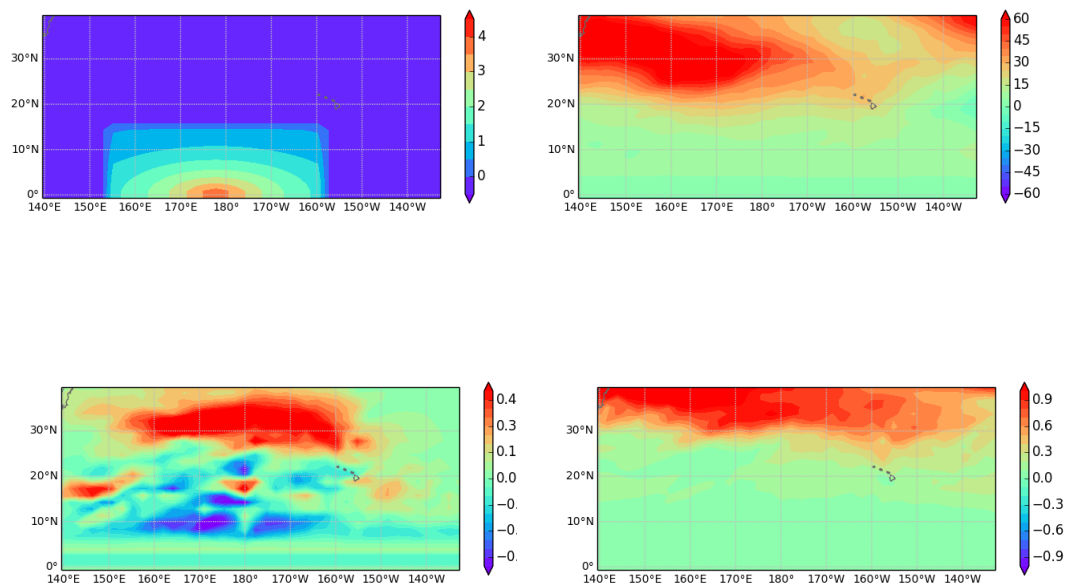


**Figure 3.** (a) Heating rate at 4000m, units  $^{\circ}\text{K day}^{-1}$ . (b) Zonal geostrophic wind units  $\text{ms}^{-1}$  at 11500m. (c) Diagnosed zonal geostrophic wind tendency at 11500m, units  $\text{ms}^{-2}$ . (d) (2,2) coefficient of  $\mathbf{BQ}'$  matrix, eq. 20, at 11500m, units  $10^8 \times \text{s}^{-2}$ .

### 3.5. Effect of boundary layer heating

A feature of the diagnostic procedure is the inclusion of a proper treatment of the boundary layer. As shown in (34), the boundary layer heating projects strongly onto the temperature, as the vertical motion is suppressed near the surface. This heating will also allow a horizontal temperature gradient to develop in the boundary layer. Since there is no horizontal pressure gradient above the boundary layer, hydrostatic balance will generate a heat low near the surface, resulting in convergence of the geotriptic wind which flows down the pressure gradient. Hence upward motion will be generated at the top of the boundary layer.

This is particularly important in the tropics, where it allows representation of the return circulation consistent with the upward motion in the deep tropics. The example shown illustrates the response to boundary layer heating over Borneo. The local time is around 1000 (0200UTC). There is

strong convergence over both Borneo and Celebes to the east, leading to upward motion (not shown), and also anticyclonic rotation..

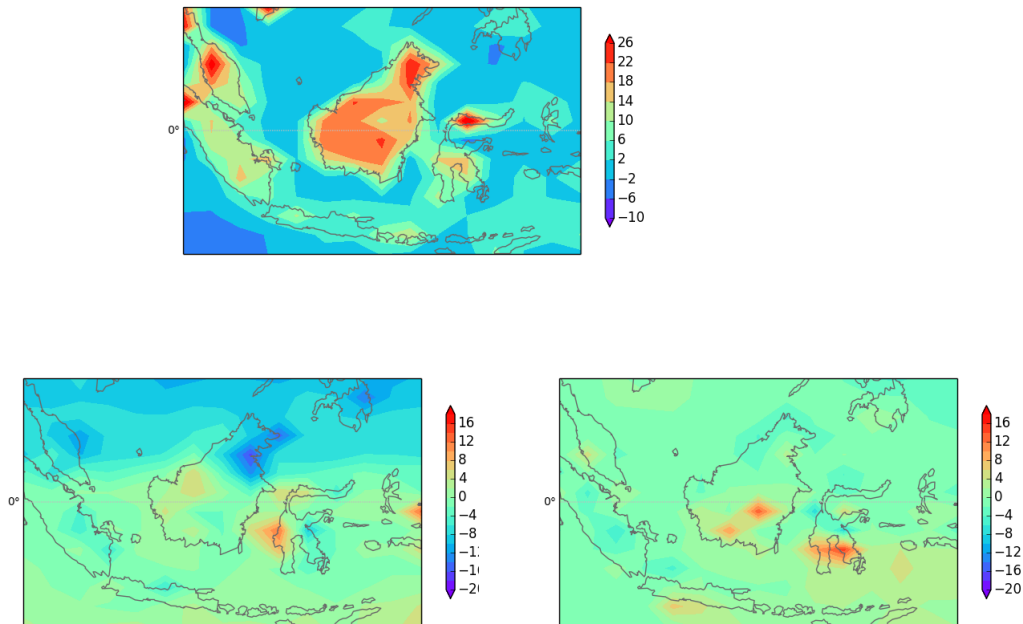


**Figure 4.** Diagnostics calculated over a region  $10^{\circ}\text{S}$  to  $10^{\circ}\text{N}$  and  $100^{\circ}\text{E}$  to  $130^{\circ}\text{E}$  at 80m height above the surface. (a) Boundary layer heating, units  $^{\circ}\text{K day}^{-1}$ ; (b) total zonal wind calculated from (19), (c) total meridional wind calculated from (19).

#### 4. Discussion

The paper has developed a diagnostic procedure based on semi-geostrophic theory that can be applied successfully to data from a comprehensive global model. It is necessary to filter the data to large horizontal scales, particularly in the tropics, as expected. This means that it can be used to extract the ‘balanced’ response to forcing, either by the model dynamics and physics, or artificially imposed forcing. The first example shows that the SGT approximation gives results which match the large-scale behaviour of the UM sufficiently closely to be useful. In particular, the predicted ageostrophic flow correlates quite well with the UM’s ageostrophic flow. Greater accuracy cannot realistically be expected given the wide range of scales and forcing mechanisms present in real and model-simulated flow. An alternative view is to say that the UM appears to reproduce the balanced response to forcing as calculated by the diagnostic.

The diagnostic should be able to aid the study of systematic errors, which usually have a large-scale signal. The predicted circulation is strongly dependent on the model state, so that errors in the resulting circulation can come from errors in the model state as well as errors in the forcing. In this application, the results of the diagnostic procedure would need to be averaged over a large number of cases, so that the noise created by using data on the borderline for applicability of SGT would be filtered out. The second example supports this by showing that much of the extratropical precipitation signal can be reproduced using the diagnosed vertical motion and the cloud fraction. This will help in identifying the causes of systematic errors in precipitation. The third example shows that the effect of tropical-extratropical interaction is strongly dependent on the background state assumed, the causes of errors in this could be distinguished by replacing the model state with a reanalysis, while still using

the same forcing. The final example shows the leading order effect of boundary layer forcing on the circulation, again allowing the causes of systematic errors to be identified.

**Conflicts of Interest:** “The author declares no conflict of interest.”

## Abbreviations

The following abbreviations are used in this manuscript:

GCM	General Circulation Model
SEE	Sawyer-Eliassen equation
SG	semi-geostrophic
SGT	semi-geotriptic
UM	Unified Model
WTG	Weak Temperature Gradient

## References

1. Beare, R.J. and Cullen, M.J.P. Diagnosis of boundary-layer circulations *Phil. Trans. R. Soc. A* **2013**, *371*, 20110474
2. Beare, R. J., and M. J. P. Cullen, Validating weather and climate models at small Rossby numbers: including a boundary layer. *Quart. J. Roy. Meteor. Soc.*, **2016**, *142* (700), 2636-2645, doi:10.1002/qj.2852.
3. Brown, A., S. Milton, M. Cullen, B. Golding, J. Mitchell, and A. Shelly. Unified modeling and prediction of weather and climate: A 25-year journey. *Bull. Amer. Meteor. Soc.* **2012**, *93* (12), 1865-1877, DOI:10.1175/BAMS-D-12-00018.1.
4. Charney J.G. On the scale of atmospheric motions. *Geophys. Publ.* **1948**, *17* no. 2,4-17.
5. Cullen, M. J. P. and M. H. Mawson. An idealised simulation of the Indian monsoon using primitive-equation and quasi-equilibrium models. *Quart. J. Roy. Meteor. Soc.* **1992** *118*, 153-164.
6. Cullen, M.J.P., R.J. Douglas, I. Roulstone. and M.J. Sewell. 2005 Generalised semi-geostrophic theory on a sphere. *J. Fluid Mech.*, **2005**, *531* 123-157.
7. Cullen, M.J.P. *A mathematical theory of large-scale atmospheric flow.*, Imperial College Press, London, UK, 2006: 259pp, ISBN 1-86094-518-X.
8. Cullen, M.J.P. Semigeostrophic solutions for flow over a ridge. *Quart. J. Roy. Meteorol. Soc.*, **2007**, *133*, 491-501.
9. Cullen, M.J.P. Analysis of the semi-geostrophic shallow water equations. *Physica D*, **2008**, *237*: 1461-1465.
10. Cheng, J., M.J.P. Cullen, and M. Feldman. Semi-geostrophic system with variable Coriolis parameter. *Arch. Rat. Mech. Anal.* **2016**, 1-58 DOI. 10.1007/s00205-017-1159-3
11. Eliassen, A. The quasi-static equations of motion with pressure as independent variable. *Geophys. Publ.* **1950**, *17* no. 3, 3-43.
12. Eliassen, A. Geostrophy. *Quart. J. Roy. Meteor. Soc.*, **1984**, *110* 1-12.
13. Hinch, E.J. *Perturbation Methods*, Cambridge University Press **1991**, ISBN 0-521-37310-7.
14. Hoskins, B.J. The mathematical theory of frontogenesis. *Ann. Rev. Fluid Mech.* **1982**, *14* 131-151.
15. Jin, F. and B. J. Hoskins The direct response to tropical heating in a baroclinic atmosphere. *J. Atmos. Sci.* **1995**, *52* 307-319.
16. Majda, A. and R. Klein. Systematic Multi-Scale Models for the Tropics. *J. Atmos. Sci.* **2003**, *60* 357-372.
17. Martin, G.M., S. F. Milton, C. A. Senior, M. E. Brooks, S. Ineson, T. Reichler, and J. Kim. Analysis and reduction of systematic errors through a seamless approach to modeling weather and climate. *J. Climate* **2010** *23* (22), 5933- 5957, DOI:10.1175/2010JCLI3541.1.
18. Matthews, A. J., B. J. Hoskins and M. Masutani. The global response to tropical heating in the Madden-Julian oscillation during the northern winter. *Quart. J. Roy. Meteorol. Soc.*, **2004**, *130*, 1991-2011.
19. Phillips, N.A.. Geostrophic motion. *Rev. Geophys.*, **1963**, *1* 123-176.
20. Schubert, W. H. Semi-geostrophic theory. *J. Atmos. Sci.* **1985**, *42* 1770-1772.
21. Schubert, W. H., P. E. Ciesieleski, D. E. Stevens and H-C Kuo. Potential vorticity modelling of the ITCZ and the Hadley circulation. *J. Atmos. Sci.* **1991** *48*, 1493-1509.
22. Sobel, A.H., J. Nilsson and L.M. Polvani 2001 The weak temperature gradient approximation and balanced tropical moisture waves. *J. Atmos. Sci.* **2001**, *58*, 3650-3665.

23. Thorpe, A. J. and Pedder, M. A. The semi-geostrophic diagnosis of vertical motion. II: Results for an idealized baroclinic wave life cycle. *Quart. J. Roy. Meteorol. Soc.* **1999**, *125*, 1257-1276.
24. White, A. A., B. J. Hoskins, I. Roulstone, and A. Staniforth, A. Consistent approximate models of the global atmosphere: shallow, deep, hydrostatic, quasi-hydrostatic and non-hydrostatic. *Quart. J. Roy. Meteorol. Soc.* **2005**, *131*, 2081-2108.
25. Wood N., A. Staniforth, A. White, T. Allen, M. Diamantakis, M. Gross, T. Melvin, C. Smith, S. Vosper, M. Zerroukat, J. Thuburn. An inherently mass-conserving semi-implicit semi-Lagrangian discretization of the deep-atmosphere global nonhydrostatic equations. *Q.J.R. Meteorol. Soc.* **2014**, *140* 1505-1520. DOI:10.1002/qj.2235.
26. Xu, Q. Extended Sawyer-Eliassen Equation for Frontal Circulations in the Presence of small Viscous Moist Symmetric Stability. *J. Atmos. Sci.* **1989**, *46*, 2671-2683. [https://doi.org/10.1175/1520-0469\(1989\)046<2671:ESEFFC>2.0.CO;2](https://doi.org/10.1175/1520-0469(1989)046<2671:ESEFFC>2.0.CO;2)